SCIENTIFIC REPORTS

OPEN

SUBJECT AREAS:
ELECTRONIC PROPERTIES AND DEVICES
SURFACES, INTERFACES AND THIN FILMS
SENSORS AND BIOSENSORS
TWO-DIMENSIONAL MATERIALS

Received
25 June 2013

Accepted
30 August 2013

Published
19 September 2013

Correspondence and requests for materials should be addressed to L.S. (slt@seu.edu.cn) or M.T. (mut11@psu.edu)

Ultrahigh humidity sensitivity of graphene oxide

Hengchang Bi[1], Kuibo Yin[1], Xiao Xie[1], Jing Ji[1], Shu Wan[1], Litao Sun[1], Mauricio Terrones[2,3] & Mildred S. Dresselhaus[4]

[1]SEU-FEI Nano-Pico Center, Key Laboratory of MEMS of Ministry of Education, Southeast University, Nanjing 210096, P. R. China, [2]Department of Physics, Department of Materials Science and Engineering Center for 2_Dimensional and Layered Materials, Pennsylvania State University, University Park, PA 16802, [3]Research Center for Exotic Nanocarbons, Shishu University, Nagano 380-8553, Japan, [4]Department of Physics and Department of Electrical Engineering and Computer Science, MIT, Cambridge, MA02139, USA.

Humidity sensors have been extensively used in various fields, and numerous problems are encountered when using humidity sensors, including low sensitivity, long response and recovery times, and narrow humidity detection ranges. Using graphene oxide (G-O) films as humidity sensing materials, we fabricate here a microscale capacitive humidity sensor. Compared with conventional capacitive humidity sensors, the G-O based humidity sensor has a sensitivity of up to 37800% which is more than 10 times higher than that of the best one among conventional sensors at 15%–95% relative humidity. Moreover, our humidity sensor shows a fast response time (less than 1/4 of that of the conventional one) and recovery time (less than 1/2 of that of the conventional one). Therefore, G-O appears to be an ideal material for constructing humidity sensors with ultrahigh sensitivity for widespread applications.

Measurement and control of environmental humidity is of great importance in industrial, agricultural, and human activities[1]. Various types of humidity sensors have been developed over the years[2]. Humidity sensors with higher sensitivity, wider humidity detection range, as well as quicker response and shorter recovery times are necessary to meet people's needs. To achieve these goals, considerable attention has been directed toward the development of humidity sensitive materials or elements, especially nanomaterials due to their high surface to volume ratio including one-dimensional (1D) carbon[3], silicon[4], ceramic[5] nanomaterials, semiconductor nanoparticles[6] and metal oxide nanowires[1,7], and nanofilms[8]. However, progress remains limited to date. Therefore, developing a novel humidity sensing material that possesses high and even sensitivity for the full range of humidity remains a challenge.

Graphene, a two-dimensional monolayer of sp^2-bonded carbon atoms exhibiting exceptional mechanical[9], thermal[10], and electrical properties[11,12], holds great potential for ultrasensitive detection. Sensors based on graphene prepared via the micromechanical cleavage of graphite[13,14] or via the reduction of graphene oxide (G-O)[15–21] have raised significant interest. These sensors show very high sensitivity to gases, including NO_2, NH_3, and so on. Sensors with single-molecule sensitivity have also been reported[13]. The mechanism of these ultrasensitive gas sensors is similar to that of carbon nanotube-based gas sensors[22–26]. Although some studies have reported water adsorption on graphene[27,28], long response time (3–5 min) hinder its applications[27]. Therefore, using this nanomaterial to fabricate humidity detection sensors remains difficult.

As an alternative graphene precursor, G-O presents considerable advantage as a material for sensing applications, especially for water detection. Graphite oxide can be used to massively produce graphene and is water dispersible, thereby enabling subsequent exfoliation into few-layer nanostructures to form G-O[15]. Thus producing continuous films from G-O suspensions is fairly straightforward[16,29–31]. The basal plane and edges of G-O platelets are composed of distributed chemical groups containing oxygen[32–34] (see Supplementary Information Fig. S1), which can increase the hydrophilicity of G-O and consequently enhance the sensitivity of the sensors to water[35]. Moreover, chemical groups can make G-O electrically insulating[36], which enables the convenient incorporation of graphene oxide into capacitive sensors. In contrast to graphite with water intercalated molecules[37], G-O more easily uptakes water vapor from the gas phase. Yao *et al.*[38] have used G-O-silicon bi-layer flexible structure as stress-based humidity sensors. This sensor exhibits a fast response time and recovery time, and a little hysteresis. However, this kind of sensors need a high working voltage (5 V), which will result in high power consumption.

Here we develop a humidity sensor using G-O as a humidity sensing material. We find that G-O–based humidity sensors can overcome the existing problems[39–46] mentioned above, and exhibit ultrahigh humidity sensitivity, as well as short response and recovery times. The humidity sensitivity of these prepared sensors reaches up to 37800% at 15%–95% relative humidity (RH). On the other hand, conventional capacitive humidity sensors have sensitivities ranging from 43% to 2900%[35,39–41,44]. The response time of our humidity sensor is 10.5 s which is 1/120 to 1/4 that of conventional humidity sensors[35,39,40,44]. The sensor also exhibits high sensitivity (1667%) which is 133 to 277 times higher than that of conventional humidity sensors even under low humidity conditions (<40%RH)[39–41,44].

Results

Fabrication of the G-O based sensor. To investigate the humidity sensing properties of G-O, a G-O based sensor (in-plane capacitor) was fabricated via a two-step procedure. The first step was to fabricate microscale interdigitated electrodes, and the detailed fabrication procedure is shown in the supplementary information Fig. S2. The next step was the fabrication of the sensor using G-O as the insulated humidity-sensing material, in which drop-casting was adopted[47]. In brief, a drop of G-O dispersion (50 μl, 1 mg/ml, dissolved in ethanol) was dropped onto the interdigitated electrodes through a pipette, followed by drying under a temperature 45°C for 1 h. Figure 1a shows the various silicon structures that exist, and the area enclosed by the red dashed lines that was used in this study. The magnified image (Fig. 1b) shows that the sensor comprises two sets of interdigital electrodes. To more comprehensively examine the humidity sensing performance of the sensor, we characterized the interdigital electrodes by scanning electron microscopy (SEM) before and after being covered with G-O films. Compared with the interdigitated electrode in Fig. 1c, that shown in Fig. 1d exhibits abundant wrinkles, demonstrating complete coverage with the G-O films (see Supplementary Information Fig. S3). It is noteworthy that this G-O film was annealed at 75°C for 24 h aiming at improving the stability of the sensor[48]. G-O sheets contain abundant oxygen-containing functional groups (see Supplementary Information Fig. S1). X-ray photoelectron spectroscopy (XPS) of G-O reveals that the carbon-to-oxygen atomic ratio (C/O) is close to 2.4, and the atomic concentration of oxygen is 29.33% (see Supplementary Information Fig. S4). In addition, thin G-O films could result in high sensitivity and fast response. Figure 1e shows the schematic diagram of the humidity testing system, in which the graphene oxide film was used as a humidity sensing material and an LCR was adopted to measure the change of capacitance of the sensors.

Performances of the sensors. In this study, the humidity-sensing performance of the G-O based sensors was tested under various levels of relative humidity (RH). Such parameters as humidity sensitivity, response time and recovery times, and stability were evaluated. Figure 2a shows the dependence of the sensor capacitance on RH at different frequencies (100 Hz, 1 kHz, and 10 kHz). The reported data are the mean values obtained from several measurement cycles at a temperature of 25°C. As the RH level increases, the output capacitance of the sensor shifts higher monotonically. Adsorbed water can increase the dielectric constant and the capacitance. More adsorbed water molecules strengthen the polarization and increase the dielectric constant[49]. Among the three frequencies, 100 Hz exhibits the best linearity. To quantitatively depict sensor sensitivity, we define it as follows[5]:

$$\text{Sensitivity} = (C_x - C_{15})/C_{15} \quad (1)$$

or

$$\text{Sensitivity} = (C_x - C_{15})/(RH_x - RH_{15}) \quad (2)$$

where C_x and C_{15} are the capacitances at x% and 15% RH levels, respectively. It can be observed from Fig. 2a and Fig. S5, that the capacitance decreased with increasing frequency. The capacitance was almost flat above 10 kHz. Thus, the capacitance became independent of the humidity with increasing frequency. This is because the electrical field direction changes slowly at low frequencies and there appears the space-charge polarization of adsorbed water. While the frequency is high, the electrical field direction changes so fast that the polarization of the adsorbed water cannot catch up with it, and hence the dielectric constant is small and independent of RH[50]. Therefore, the sensitivity defined in equation (2) decreases with increasing the frequency. Figure 2b demonstrates the relationship between sensitivity defined in equation (1) and RH. Obviously, the sensitivity at 1 kHz is higher than that at the two other frequencies. When the RH level changes from 15% RH to 95% RH, the capacitance rises from 9.8 pF to

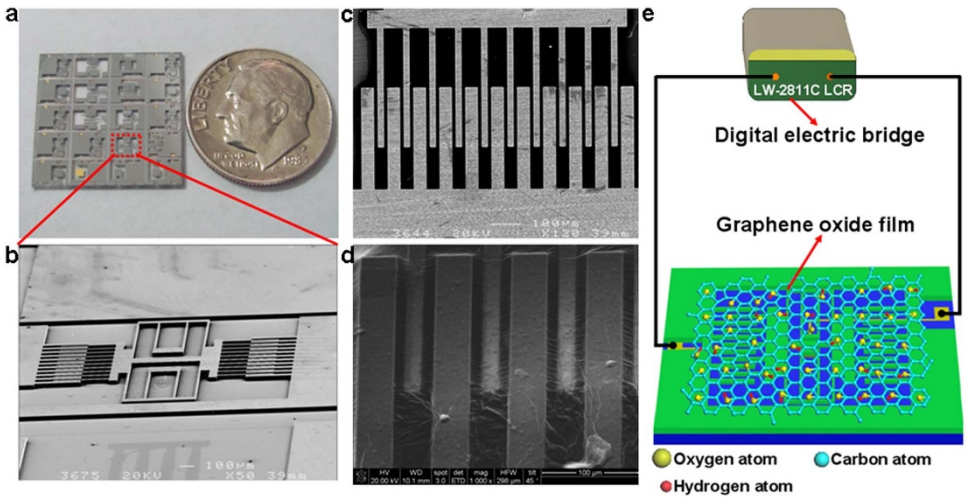

Figure 1 | Characterization of the sensor and humidity testing system. (a): Digital photographs of the device (Reference is a 1 Dime US coin). (b): SEM image of the area set off by a red dashed line. (c): SEM image of the interdigitated electrodes without G-O. Two sets of electrodes (with widths of 40 and 20 μm, respectively) were designed in an interdigitated manner with 10 μm spacing and an overlapping area of 200 μm. (d): SEM image of interdigitated electrodes covered with G-O films. (e): Schematic diagram of the humidity testing system graphene oxide film as a humidity sensing material was placed on the two sets of interdigitated electrodes.

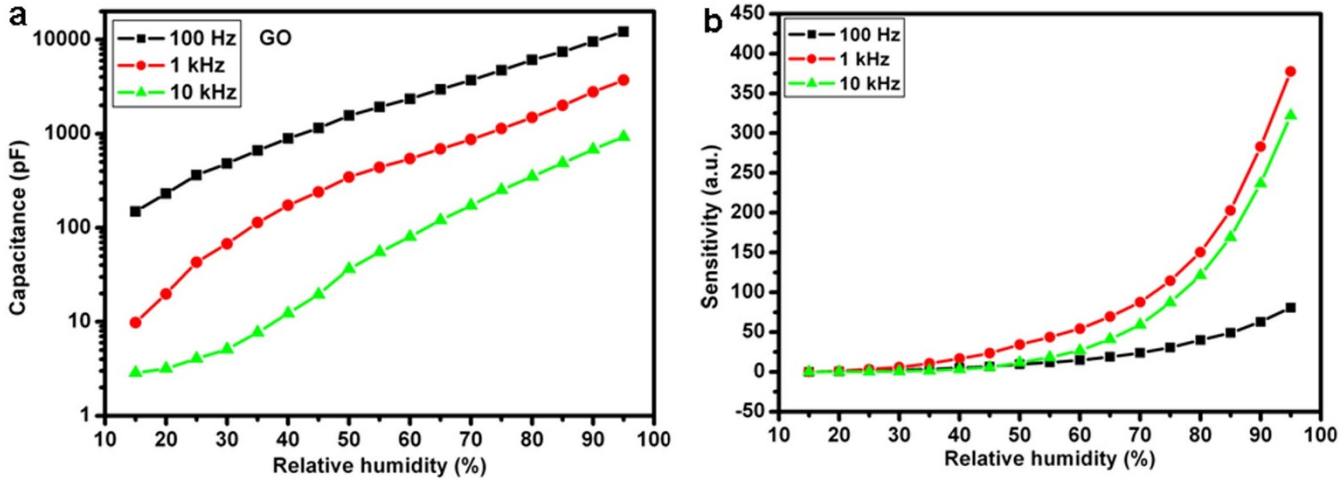

Figure 2 | Capacitance and sensitivity versus RH at 100 Hz, 1 kHz, and 10 kHz. (a): Output capacitances of sensors as a function of RH. (b): Defined sensitivity as a function of RH.

3710 pF, and the corresponding relative capacitance change is 37800%. By contrast, the relative capacitance changes for 100 Hz and 10 kHz are 8000% and 32200%, respectively. These values are significantly higher than those of capacitive humidity sensors based on other materials[35,39–41,44] at the same conditions. Therefore, 100 Hz and 1 kHz are selected as the operating frequencies in our experiments.

Stability is an important parameter of humidity-sensing properties. The sensor was tested repeatedly under fixed humidity levels (15%, 35%, 55%, 75%, and 95% RH) in a period of 30 days. The results are shown in Fig. 3. The capacitance variation is less than 4% at each humidity region for one month at 100 Hz and less than 6% at each humidity region for one month at 1 kHz, which shows the output capacitances of the sensor operating at 100 Hz and 1 kHz fluctuate slightly with time, and the data show good consistency. Moreover, the in-plane capacitor has better stability than the sandwich-structured capacitor[51].

Both response and recovery times significantly affect the performance of humidity sensors. Response and recovery times of sensors affect the RH-increasing and RH-decreasing processes with RH ranging from 23% to 86% (Fig. 4). According to the recorder, the sensor response time (humidification from 23% RH to 86% RH) was ~10.5 s, and the recovery time (desiccation from 86% RH to 23% RH) was ~41 s, both better than conventional capacitive sensors utilizing multi-wall carbon nanotubes, silicon nanowires, macroporous silicon, anodic aluminum oxide, and so on (11% RH to 86% RH, response time 45 s; 11.3% RH to 93% RH, response time 132 s; 0% RH to 100% RH, response time 20 min; 30% RH to 95% RH, response time 188 s)[35,39,40,44]. The excellent response and recovery times are not only ascribed to the abundant hydrophilic functional groups on G-O sheets, but also to the large interlayer space in the G-O films which facilitates water adsorption and desorption. In addition, we also measured the hysteresis of the films which is close to 5% (see Supplementary Information Fig. S6).

Discussion

The electrical response of sensing materials to humidity is related to the physical adsorption of water molecules. To interpret the relationship between the capacitance and the RH, the following equation (3) was adopted to depict the relationship[41]

$$C = (\varepsilon_\gamma - i\gamma/\omega\varepsilon_0)C_0 \tag{3}$$

where γ denotes the conductance, and ω denotes frequency. According to this expression, the capacitance of the sensing material is proportional to γ, and C is inversely proportional to frequency ω. In addition, γ is related to the physisorption of water molecules on a G-O film in that different sorption processes yield different γ values. According to the literature[41], γ increases with rising RH, such that the capacitance increases with rising RH, depending on the frequency. At low RH, water molecules are primarily physisorbed onto the

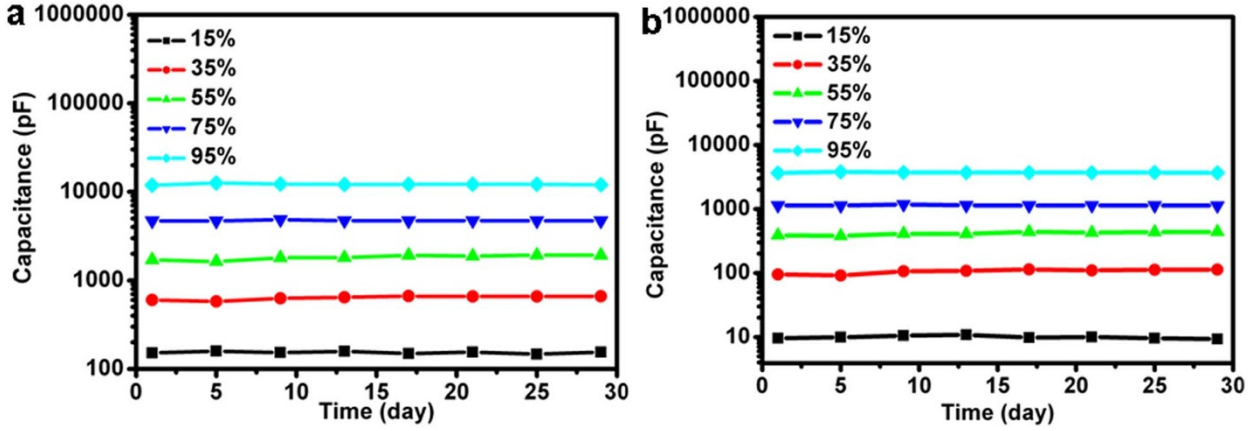

Figure 3 | Stability test of sensors at fixed RH. (a): 100 Hz. (b): 1 kHz. The change in the output capacitance of sensors operating at 100 Hz and 1 kHz was acceptable, that is, long-term stability and reliability are beneficial for practical applications.

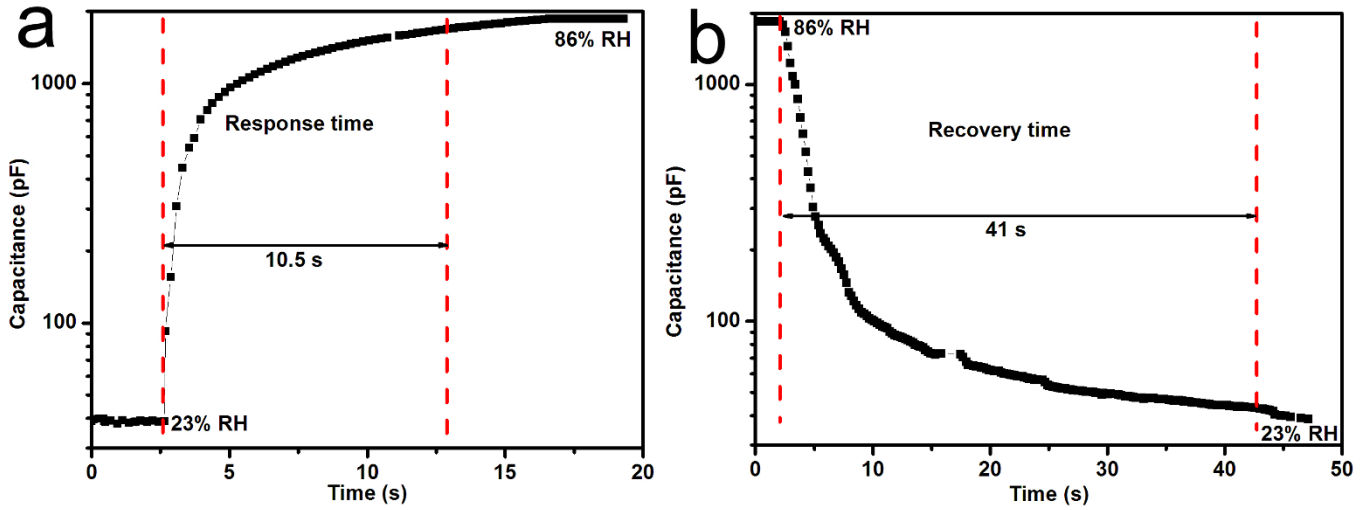

Figure 4 | Response and recovery times of the humidity sensors for humidity levels between 23% RH and 86% RH. (a): Response time, ~10.5 s. (b): Recovery time, ~41 s.

available active sites (hydrophilic groups, vacancies) of the G-O surface through double hydrogen bonding, which is called the first-layer physisorption of water (Fig. 5). In this regime, the water molecules are thus unable to move freely because of the restriction from double hydrogen bonding. The hopping transfer of protons between adjacent hydroxyl groups in the first-layer physical adsorption of water requires much energy, and for this reason G-O films exhibit strong electrical resistance. Although the protons in G-O films are minimal, and are restricted by discontinuous mobile layers, they contribute to the leak conduction γ[41], which essentially increases the capacitance at low RH. As the RH increases, the multilayer physical adsorption of water molecules (Fig. 5) occurs. From the second physisorbed layer, water molecules are physisorbed through single hydrogen bonding on the hydroxyl groups. Thereafter, the water molecules become mobile and progressively more identical to those in the bulk liquid. As the multilayer physical adsorption progresses, the physisorbed water can be ionized under an electrostatic field to produce a large number of hydronium ions (H_3O^+) as charge carriers. With further increase in humidity, the physisorbed water layers gradually exhibit liquid-like behavior. In bulk liquid, proton hopping between adjacent water molecules occurs in G-O, with charge transport taking place via the conductivity generated by a Grotthuss chain reaction ($H_2O + H_3O^+ \rightarrow H_3O^+ + H_2O$) conductivity[52], which can cause an increase of γ. In addition, at high RH, the physisorbed water will penetrate into the interlayer of G-O films (see Supplementary Information, Fig. S1), which is very beneficial for the hydrolysis of the functional groups (carboxyl, sulphonic, and/or hydroxyl) on G-O sheets, and these ions contribute to the ionic conductivity[51]. The large number of existing epoxy groups in G-O could aid proton migration. All of these factors would lead to a sudden increase of γ, which is consistent with the tendency shown in figure 2, leading to a quite high sensitivity at high RH. In addition, the dielectric constants of water under different conditions vary. For instance, the dielectric constant of hydrated water at low RH is 2.2, that of free water at high RH is 78. This variance enhances sensor capacitance, thereby resulting in high sensitivity. This finding explains the excellent humidity-sensing characteristics of G-O.

To confirm the different sorption mechanisms of sensing materials at various RH values, complex impedance spectra are adopted to interpret the conductivity and polarization processes that take place in a humidity sensor. Typical complex impedance spectra of the sensor at different RH values were measured over a frequency range

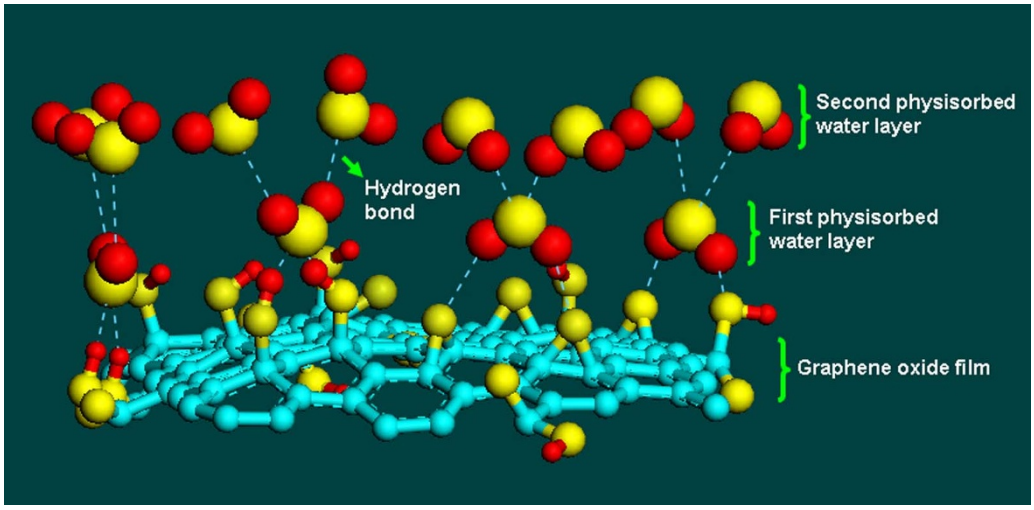

Figure 5 | Schematic of humidity sensing at G-O films. The adsorption of water molecules on G-O films is characterized by two processes. The first-layer water molecules are attached on the G-O films through two hydrogen bonds. In contrast, from the second layer, water molecules are adsorbed only through one hydrogen bond.

of 20 Hz to 1 MHz with a testing voltage of 1 V and temperature of 15°C. The difference in the impedance spectra implies different physical phenomena for the electrical conductivity and polarization that occur in G-O in the presence of water molecules. Figure 6a shows that when RH is low (13% RH), a half semicircle is observed in the complex impedance plot. When RH in Fig. 6a increases unceasingly (33%, 53%, 75%, and 87% RH), a line appears at larger RH values, above which the semicircular behavior is finished as RH increases. The semicircular behaviors in the low frequency range are depressed. Moreover, higher RH results in a more pronounced linear behavior in Fig. 6a. When the RH increases to 97%, the semicircle becomes invisible. The semicircle is typical of the relaxation

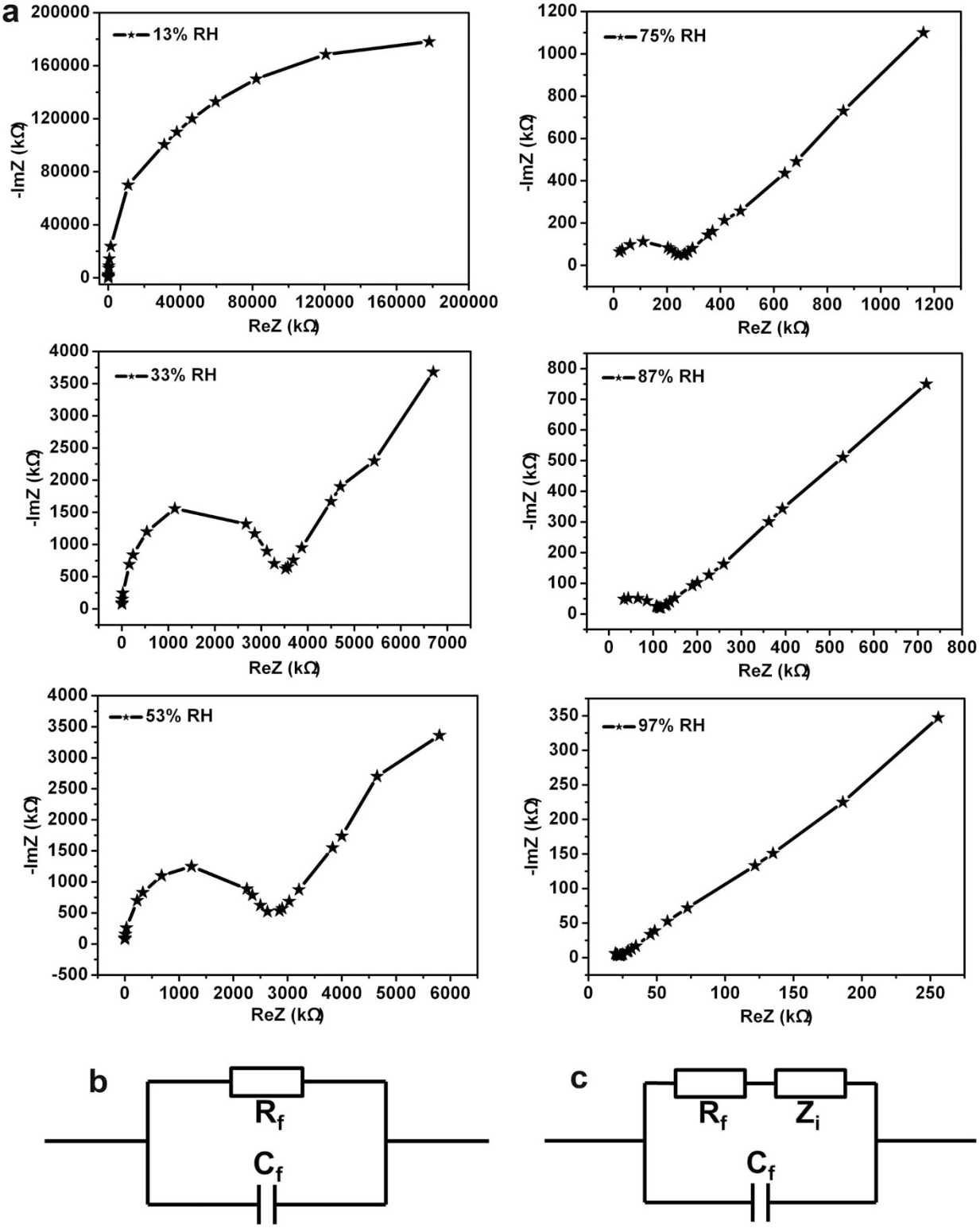

Figure 6 | Complex impedance plots and equivalent circuits of G-O films under different humidity levels. (a): With increasing RH, the semicircles are gradually depressed and then disappear at 97% RH. The straight lines become lengthened. (b): An equivalent circuit at very low RH. (c): An equivalent circuit at high RH. R_f: G-O film resistance; C_f: G-O film capacitance; Z_i: interface impedance between G-O film and electrodes.

mechanism exhibited by resistance–capacitance parallel circuits. Therefore, the semicircle results primarily from the intrinsic impedance of the sensing film. The decrease in the curvature of the semicircle with increasing RH reflects the decrease in the intrinsic impedance, which is related to the interaction between the sensing film and water. The physical phenomena of the electrical conductivity and polarization that occur in a humidity sensor are represented not only by resistances and capacitances, but also by the diffusion and interface phenomena of ions. The straight line may stem from the ionic and/or electrolytic conductivity.

G-O films not only have high surface-to-volume ratios, but also possess a large density of surface vacancies and hydrophilic functional groups resulting from violent oxidation (see supplementary information Fig. S1 and Fig. S4), thus increasing sensor sensitivity[35]. The resistance of this material is extremely high[51], so that inducing electrical conductivity in a dry ambient environment is difficult to accomplish. Therefore, the electronic conductivity of G-O films themselves is inconspicuous, and the mechanism governing such conductivity depends on the surface coverage of adsorbed water. At very low RH levels (13%), the water vapor is minimal. Hence, the concentration of the adsorbed water is low. Where the first-layer physical adsorption occurs, it is different from the chemisorption process (and is unaffected by further changes in humidity). So first-layer adsorption can be used to explain the high sensitivity even at low RH. With the increase of humidity within the low RH range, more and more water molecules are adsorbed and form the first-layer physical adsorption through double hydrogen bonding, which will be responsible for the rise in the capacitance upon the application of an electric field.

The complex impedance plot of Fig. 6a can be modeled by equivalent circuits, as shown in Fig. 6b and Fig. 6c. The semicircle plot of the impedance represents a kind of sensing mechanism, which can be modeled by an equivalent parallel circuit of a resistor and capacitor[53,54], as shown in Fig. 6b. The curve of semicircle connected with a line represents another kind of sensing mechanism, of which the equivalent circuit has been also shown in Fig. 6c[53,54]. Here R_f represents the resistance of the G-O film, which decreases as RH increases; C_f the capacitance of the G-O film and Z_i the impedance at the electrodes/G-O film. At very low RH, the resistor is related to H_3O^+, and the capacitor is related to proton conductivity. As RH increases, more water molecules are physisorbed into this hydroxyl layer on the large specific surface area of G-O films. Additionally, a high local charge density and a strong local electrostatic field exist in the surface defects, promoting the dissociation of water physisorbed on the surfaces of G-O films. Thus, proton hopping between adjacent water molecules occurs easily in G-O, with charge transport via the conductivity induced by a Grotthuss chain reaction ($H_2O + H_3O^+ \rightarrow H_3O^+ + H_2O$)[51], which causes the decrease of the intrinsic resistance of the G-O film corresponding to the more depressed semicircles and longer straight lines in Fig. 6a at higher RH values. With the increase of humidity, the functional groups on the G-O film are hydrolyzed partly leading to the result that the semicircles depress further and the straight lines become increasingly longer. Until a humidity up to 97% RH, the electrolytic conductivity dominates over protonic conductivity, that is, the functional groups on G-O are hydrolyzed mostly or even totally, the semicircle is invisible and only the straight line is left, as indicated in Fig. 6a. As a result, the resistance and the capacitance of the sensor at high RH are primarily attributed to the decomposition and orientation polarization of physisorbed water and active functional groups on G-O.

A novel capacitive-type humidity sensor based on G-O has been presented in this work. A large number of hydrophilic groups, including carboxyl groups, hydroxyl groups, and so on, as well as vacancies on G-O plates, endow G-O with excellent humidity-sensing behavior. Electrical testing under different RH environments shows that the sensor based on G-O exhibits ultrahigh sensitivity (37800% at 1 kHz) over the entire RH range. Furthermore, the sensor shows excellent performance along with rapid response and recovery times, relatively low hysteresis, and excellent stability. We also established a mechanism that can potentially explain the excellent performance of the G-O-made sensors.

Methods

Preparation of graphite oxide (GO). GO was prepared by oxidizing expandable graphite (EG) powder based on the Hummers method[55]. Details are described as follows: EG powder (2 g) and sodium nitrate (1 g) were mixed with sulfuric acid (46 ml, 98 wt%) in an ice bath. Potassium permanganate (6 g) was slowly added to the mixture to prevent the temperature from exceeding 20°C. The reaction was maintained at 35°C ± 1°C for 8 h with gas release. Deionized water (92 ml) was gradually added, resulting in violent effervescence. The temperature of the water bath was increased to 98°C, and the reaction was maintained for 2 h to increase the degree of oxidation of the G-O product. The resultant bright-yellow suspension was diluted with deionized water (280 ml) and further treated with a H_2O_2 solution (6 ml, 30%). The product was separated by centrifugation and washed seven times with 5% hydrochloric acid solution until the sulphate could no longer be detected with $BaCl_2$. The product was washed seven times with distilled water to remove chloride ions and then dried overnight in an air oven at 60°C.

Characterization. The X-ray diffraction patterns of the G-O (from 5° to 60°) were measured using an Arl X'TRA diffractometer with an output power of 2.2 kW. G-O sheets were filtrated and purified several times and then ground to powder using a mortar andpestle. Infrared spectroscopy (400 to 4000 cm^{-1}) was performed using a Nicolet IR 870 FTIR spectrometer with pure KBr as the background. Repetitive filtrations were conducted before grinding the sheets with KBr for sample preparation. The ground powder was then dried and shaped into a transparent tablet for measurement.

Measurements of various parameters including sensitivity, stability, response time, and recovery time of G-O. The sensitivity and stability of G-O-based sensors were investigated using a Climatic Test Chamber (C, 340, −70) with an accurate control module (OMEG 205). To summarize, the capacitance of the capacitors and sensors was measured using a LW-2811C LCR meter at 25°C. The frequencies used were 100 Hz, 1 kHz, and 10 kHz. The humidity sensor was then placed in a Climatic Test Chamber (C, 340, −70) with an accurate control module (OMEG 205) for 40 min to allow the humidity sources to reach an equilibrium state. To estimate the response time and recovery times, atmospheres with RH of 23% and 86% were achieved by saturated aqueous solutions of CH_3COOK and KCl at temperature of 25°C[35], respectively. The response and recovery times between 23% RH and 86% RH were measured by transferring the sensors from a closed glass vessel to another closed glass vessel. The time spent in reaching 90% of the capacitance change was denoted as the response and recovery time. The performance of the sensor was measured every 3 days to monitor its stability.

Complex impedance spectra for different RHs were obtained through use of a TH2828S LCR meter with testing voltage of 1 V and temperature of 15°C. To set up different RH environments, saturated aqueous of LiCl, $MgCl_2$, $Mg(NO_3)_2$, NaCl, KCl, and K_2SO_4 were placed in airtight glass vessels at a temperature of 15°C, which yielded atmospheres with RHs of 13%, 33%, 53%, 75%, 87%, and 97%[1,56].

1. Li, Z. Y. *et al*. Highly sensitive and stable humidity nanosensors based on LiCl doped TiO_2 electrospun nanofibers. *J. Am. Chem. Soc.* **130**, 5036–5037 (2008).
2. Lee, C. & Lee, G. Humidity sensors: A Review. *Sens. Lett.* **3**, 1–15 (2005).
3. Zilberman, Y., Lonescu, R., Feng, X. L., Müllen, K. & Haick, H. Nanoarray of polycyclic aromatic hydrocarbons and carbon nanotubes for accurate and predictive detection in real-world environmental humidity. *ACS Nano* **5**, 6743–6753 (2011).
4. Chen, X. J., Zhang, J., Wang, Z. L., Yan, Q. & Hui, S. C. Humidity sensing behavior of silicon nanowires with hexamethyldisilazane modification. *Sens. Actuators, B* **156**, 631–636 (2011).
5. Kim, Y. *et al*. Capacitive humidity sensor design based on anodic aluminum oxide. *Sens. Actuators, B* **141**, 441–446 (2009).
6. Demir, R., Okur, S. & Şeker, M. Electrical characterization of CdS nanoparticles for humidity sensing applications. *Ind. Eng. Chem. Res.* **51**, 3309–3313 (2012).
7. Kuang, Q., Lao, C. S., Wang, Z. L., Xie, Z. X. & Zheng, L. S. High-sensitivity humidity sensor based on a single SnO_2 nanowire. *J. Am. Chem. Soc.* **129**, 6070–6071 (2007).
8. Zhang, Y. S., Yu, K., Jiang, D. S., Zhu, Z. Q., Geng, H. R. & Luo, L. Q. Zinc oxide nanorod and nanowire for humidity sensor. *Appl. Surf. Sci.* **242**, 212–217 (2005).
9. Frank, I. W., Tanenbaum, D. M., Van der Zande, A. M. & McEuen, P. L. Mechanical properties of suspended graphene sheets. *J. Vac. Sci. Technol., B* **25**, 2558–2561 (2007).
10. Balandin, A. A. *et al*. Superior thermal conductivity of single-layer graphene. *Nano Lett.* **8**, 902–907 (2008).
11. Geim, A. K. & Novoselov, K. S. The rise of graphene. *Nat. Mater.* **6**, 183–191 (2007).

12. Novoselov, K. S. *et al.* Electric field effect in atomically thin carbon films. *Science* **306**, 666–669 (2004).
13. Schedin, F. *et al.* Detection of individual gas molecules adsorbed on graphene. *Nat. Mater.* **6**, 652–655 (2007).
14. Cheng, Z. G., Li, Q., Li, Z. J., Zhou, Q. Y. & Fang, Y. Suspended graphene sensors with improved signal and reduced noise. *Nano Lett.* **10**, 1864–1868 (2010).
15. Ruoff, R. Calling all chemists. *Nat. Nanotechnol.* **3**, 10–11 (2008).
16. Gilje, S., Han, S., Wang, M., Wang, K. L. & Kaner, R. B. A chemical route to graphene for device applications. *Nano Lett.* **7**, 3394–3398 (2007).
17. Robinson, J. T., Perkins, F. K., Snow, E. S., Wei, Z. Q. & Sheehan, P. E. Reduced graphene oxide molecular sensors. *Nano Lett.* **8**, 3137–3140 (2008).
18. Lu, G. H. *et al.* Toward practical gas sensing with highly reduced graphene oxide: A new signal processing method to circumvent run-to-run and device-to-device variations. *ACS Nano* **5**, 1154–1164 (2011).
19. Fowler, J. D. *et al.* Practical chemical sensors from chemically derived graphene. *ACS Nano* **3**, 301–306 (2009).
20. Dua, V. *et al.* All-organic vapor sensor using inkjet-printed reduced graphene oxide. *Angew. Chem. Int. Ed.* **49**, 2154–2157 (2010).
21. Lu, G. H., Ocola, L. E. & Chen, J. H. Gas detection using low-temperature reduced graphene oxide sheets. *Appl. Phys. Lett.* **94**, 083111 (2009).
22. Kong, J. *et al.* Nanotube molecular wires as chemical sensors. *Science* **287**, 622–625 (2000).
23. Chang, H., Lee, J. D., Lee, S. M. & Lee, Y. H. Adsorption of NH_3 and NO_2 molecules on carbon nanotubes. *Appl. Phys. Lett.* **79**, 3863–3865 (2001).
24. Zhao, J. J., Buldum, A., Han, J. & Lu, J. P. Gas molecule adsorption in carbon nanotubes and nanotube bundles. *Nanotechnology* **13**, 195–200 (2002).
25. Qi, P. *et al.* Toward large arrays of multiplex functionalized carbon nanotube sensors for highly sensitive and selective molecular detection. *Nano Lett.* **3**, 347–351 (2003).
26. Novak, J. P. *et al.* Nerve agent detection using networks of single walled carbon nanotubes. *Appl. Phys. Lett.* **83**, 4026–4028 (2003).
27. Ghosh, A., Late, D. J., Panchakarla, L. S., Govindaraj, A. & Rao, C. N. R. NO_2 and humidity sensing characteristics of few-layer graphenes. *J. Exp. Nanosci.* **4**, 313–322 (2009).
28. Sreeprasad, T. S. *et al.* Electron-tunneling modulation in percolating network of graphene quantum dots: fabrication, phenomenological understanding, and humidity/pressure sensing applicatioins. *Nano Lett.* **13**, 1757–1763 (2013).
29. Wang, X., Zhi, L. & Mullen, K. Transparet, conductive graphene electrodes for dye-sensitized cells. *Nano Lett.* **8**, 323–327 (2008).
30. Becerril, H. A. *et al.* Evaluation of solution-processed reduced graphene oxide films as transparent conductors. *ACS Nano* **2**, 463–470 (2008).
31. Eda, G., Fanchini, G. & Chhowalla, M. Large-area ultrathin films of reduced graphene oxide as a transparent and flexible electronic material. *Nat. Nanotechnol.* **3**, 270–274 (2008).
32. Cai, W. W. *et al.* Synthesis and solid-state NMR structure characterization of C 13 labeled graphite oxide. *Science* **321**, 1815–1817 (2008).
33. Lerf, A., He, H. Y., Forster, M. & Klinowski, J. Structure of graphite oxide revisited. *J. Phys. Chem. B* **102**, 4477–4482 (1998).
34. He, H. Y., Klinowski, J., Forster, M. & Lerf, A. A new structural model for graphite oxide. *Chem. Phys. Lett.* **287**, 53–56 (1998).
35. Chen, W. P., Zhao, Z. G., Liu, X. W., Zhang, Z. X. & Suo, C. G. A capacitive humidity sensor based on multi-wall carbon nanotubes (MWCNTs). *Sensors* **9**, 7431–7444 (2009).
36. Park, S. & Ruoff, R. S. Chemical methods for the production of graphenes. *Nat. Nanotechnol.* **4**, 217–224 (2009).
37. Collignon, B., Hoang, P. N. M., Picaud, S. & Rayez, J. C. Ab ignition study of the water adsorption on hydroxylated graphite surfaces. *Chem. Phys. Lett.* **406**, 430–435 (2005).
38. Yao, Y., Chen, X. D., Guo, H. H., Wu, Z. Q. & Li, X. Y. Humidity sensing behaviors of graphene oxide-silicon bi-layer flexible structure. *Sens. Actuator B* **161**, 1053–1058 (2012).
39. Chen, X. J., Zhang, J., Wang, Z. L., Yan, Q. & Hui, S. C. Humidity sensing behavior of silicon nanowires with hexamethyldisilazane modification. *Sens. Actuators, B* **156**, 631–636 (2011).
40. Wang, Y., Park, S., Yeow, J. T. W., Langner, A. & Müller, F. A capacitive humidity sensor based on ordered macroporous silicon with thin film surface coating. *Sens. Actuators, B* **149**, 136–142 (2010).
41. Wang, Z. Y. *et al.* The sol-gel template synthesis of porous TiO_2 for a high performance humidity sensor. *Nanotechnology* **22**, 275502 (9) (2011).
42. Li, Y., Hong, L. J. & Yang, M. J. Crosslinked and quaternized poly (4-vinylpyridine)/polypyrrole composite as a potential candidate for the detection of low humidity. *Talanta* **75**, 412–417 (2008).
43. Sun, A. H., Li, Z. X., Wei, T. F., Li, Y. & Cui, P. Highly sensitive humidity sensor at low humidity based on the quaternized polypyrrole composite film. *Sens. Actuators, B* **142**, 197–203 (2009).
44. Kim, Y. *et al.* Capacitive humidity sensor design based on anodic aluminum oxide. *Sens. Actuators, B* **141**, 441–446 (2009).
45. Li, P., Li, Y., Yang, B. Y. & Yang, M. J. Electrospun nanofibers of polymer composite as a promising humidity sensitive material. *Sens. Actuators, B* **141**, 390–395 (2009).
46. Parthibavrman, M., Hariharan, V. & Sekar, C. High-sensitivity humidity sensor based on SnO_2 nanoparticles synthesized by microwave irradiation method. *Mater. Sci. Eng., C* **31**, 840–844 (2011).
47. Cho, E. S. *et al.* Ultrasensitive detection of toxic cations through changes in the tunneling current across films of striped nanoparticles. *Nat. Mater.* **11**, 978–985 (2012).
48. Kim, S. *et al.* Room-temperature metastability of multilayer graphene oxide films. *Nat. Mater.* **11**, 544–549 (2012).
49. Cheng, B. H., Tian, B. X., Xie, C. C., Xiao, Y. H. & Lei, S. J. Highly sensitive humidity sensor based on amorphous Al_2O_3 nanotubes. *J. Mater. Chem.* **21**, 1907–1912 (2011).
50. Pokhrel, S. M. & Nagaraja, K. S. Electrical and humidity sensing properties of chromium oxide-tungsten oxide composites. *Sens. Actuators B* **92**, 144–150 (2003).
51. Gao, W. *et al.* Direct laser writing of micro-supercapacitors on hydrated graphite oxide films. *Nat. Nanotechnol.* **6**, 496–500 (2011).
52. Agmon, N. The Grotthuss mechanism. *Chem. Phys. Lett.* **244**, 456–462 (1995).
53. Song, X. F., Qi, Q., Zhang, T. & Wang, C. A humidity sensor based on KCl-doped SnO_2 nanofibers. *Sens. Actuators, B* **138**, 368–373 (2009).
54. Su, M. Y. & Wang, J. Preparation and humidity sensitivity if multi-layered Zirconia thin films by sol-gel method. *Sens. Lett.* **9**, 670–674 (2011).
55. Hummers, W. S. & Offeman, R. E. Preparation of graphite oxide. *J. Am. Chem. Soc.* **80**, 1339–1339 (1958).
56. Zhao, Z. G., Liu, X. W., Chen, W. P. & Li, T. Carbon nanotubes humidity sensor based on high testing frequencies. *Sens. Actuators, A* **168**, 10–13 (2011).

Acknowledgements

This work was supported by the National Basic Research Program of China (Grant Nos. 2011CB707601 and 2009CB623702), the National Natural Science Foundation of China (Nos. 61274114, 51071044 and 61106055), and Program for New Century Excellent Talents in University (No. NCEF-09-0293). MT was partially supported by an AFOSR MURI (FA9550-12-1-0471).

Author contributions

L.S. and M.T. proposed and supervised the project, H.B. and K.Y. designed the experiments, H.B., J.J. and S.W. performed the experiments, L.S., M.T., M.S.D., X.X. and H.B. analyzed data and wrote the manuscript, and all the authors participated in discussions of the research.

Additional information

Supplementary information accompanies this paper at http://www.nature.com/scientificreports

Competing financial interests: The authors declare no competing financial interests.

How to cite this article: Bi, H. *et al.* Ultrahigh humidity sensitivity of graphene oxide. *Sci. Rep.* **3**, 2714; DOI:10.1038/srep02714 (2013).